JOC The Journal of Organic Chemistry

Article

pubs.acs.org/joc

Medium Effects on the 1,3-Dipolar Cycloaddition of Pyridazinium Dicyanomethanide with Ethyl Vinyl Ketone in Pure and Mixed Solvents from QM/MM Simulations

Xin Yang and Ying Xue*

College of Chemistry, Key Lab of Green Chemistry and Technology in Ministry of Education, Sichuan University, Chengdu 610064, People's Republic of China

Supporting Information

ABSTRACT: The 1,3-dipolar cycloaddition reaction between pyridazinium dicyanomethanide **1** and ethyl vinyl ketone (EVK) has been reported to be a concerted mechanism based on gas-phase ab initio calculations. Our current investigation of this 1,3-dipolar cycloaddition reaction in water, methanol, acetonitrile, H_2O-CH_3CN, and CH_3OH-CH_3CN mixtures using novel two-dimensional potentials of mean force (2-D PMF) calculations coupled to QM/MM simulations predicts an alternative free energy surface that supports a stepwise mechanism. The results for the kinetic effect are uniformly in close accord with experimental data and reflect a trigger point for the exponential rate rise in water–acetonitrile mixture. When methanol replaced water, the rate enhancements are more gradual, and there is no trigger point. Calculations in pure solvents and their mixtures at 25 °C and with pure water and acetonitrile at 37 °C indicate that the secondary bridging H-bonding from the first water molecules is necessary for the exponential rate enhancements, which is strong supported by the experimental results. This work provides new insight into solvent effects on 1,3-dipolar cycloaddition reaction.

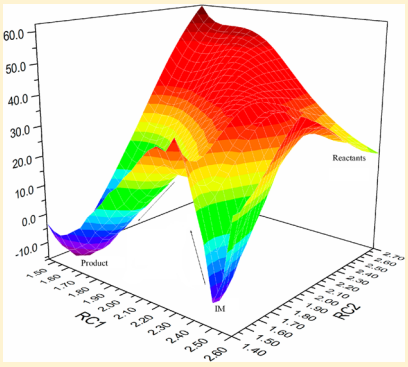

1. INTRODUCTION

Since the early work of Breslow[1,2] on the influence of water on the Diels–Alder, the use of aqueous media for organic chemical synthesis has attracted a great deal of interest. In recent years, this has been immensely amplified by environmental and cost considerations.[3] Developing an understanding of organic reactions in water has become a field of intense study.[3,4] Extensive kinetic measurements on the rates of Diels–Alder reactions in water relative to organic solvents have been reported, and they have given rise to increasing knowledge of the solvent effect of water in organic reaction.[2,5] Unlike the Diels–Alder reaction, only in the last 10 years has there been a focus on aqueous 1,3-dipolar cycloaddition reactions.[6−12]

Recently, Butler et al. have noted[13,14] that the introduction of water as cosolvent into cycloaddition reactions of the 1,3-dipole pyridazinium dicyanomethanide **1** with the dipolarophile ethyl vinyl ketone (EVK) (see Scheme 1) in acetonitrile gave small initial rate increases followed by remarkable exponential rate enhancements as the solvent mixture approached pure water.

Scheme 1. 1,3-Dipolar Cycloaddition Reaction between 1,3-Dipole Pyridazinium Dicyanomethanide 1 and Ethyl Vinyl Ketone (EVK)

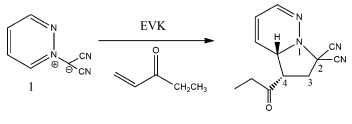

As the mole fraction of water surpassed ca. 0.9, exponential rate enhancements were triggered. When methanol replaced water, the rate increase was more gradual and no triggering effect was observed. The dramatic rate enhancement triggered for the EVK dipolarophile was significantly reduced as the temperature was raised in the range 29–64 °C. The authors thought the primary hydrogen-bonding (H-bonding) of solvent O–H groups to the transition state was rate enhancing, but secondary bridging H-bonding from the primary water-solvation shell was necessary for the exponential rate increases. Similar exponential rate plots have been reported in the cycloaddition of CN-diphenylnitrone with dibutyl fumarate.[15] Experimental kinetic and thermodynamic properties have been published for this type of reactions. However, it is unclear why different proton solvents can cause such a big difference in rate and what internal factors affect the presence of trigger point.

To further investigate the dramatic kinetic effects of 1,3-dipolar cycloaddition at the atomic level, we have explored the reaction of the 1,3-dipole **1** with the dipolarophile ethyl vinyl ketone (EVK) (see Scheme 1) and explained the medium factors which influence the shape of these plots. Mixed quantum and molecular mechanical (QM/MM)[16−18] calculations using Monte Carlo (MC) simulations and the free energy perturbation (FEP) theory have been carried out in water–acetonitrile and methanol–acetonitrile mixtures with various mole fractions of water/methanol to fully parallel the

Received: January 24, 2014
Published: April 23, 2014

   dx.doi.org/10.1021/jo500184f | J. Org. Chem. 2014, 79, 4863−4870

experimental study of Butler.[14] The reacting system has been treated using the semiempirical PDDG/PM3 method[19−21] with complete sampling of geometry of the reacting systems and explicit representation of the solvent components. This method has been tested and given excellent results in reproducing experimental solvent effects in various solvents[22−26] and reactions such as the S_N2 reaction,[27] nucleophilic aromatic substitution reaction,[28] decarboxylations,[29,30] Diels−Alder reaction,[31] and claisen rearrangement.[32] The QM/MM/MC is a well-established method for the calculation of free energy of activation ($\Delta G^{\ddagger}$) for chemical reactions, and its explicit solvation approach is a robust way of calculating accurate solvation free energies with explicit solute−solvent interactions and can provide the atomic-level structural details for characterization of the nature of the 1,3-dipolar cycloadditions. The results herein have wider implications than for the reaction investigated.

2. COMPUTATIONAL METHODS

Butler et al.[14] measured the rates for cycloaddition reaction of **1** with EVK in methanol−acetonitrile and water−acetonitrile mixtures. To gain further insight into the effect of solvent on the 1,3-dipolar cycloaddition, new binary solvent boxes were constructed in a technically similar study for the decarboxylation of a biotin model.[30] Water−acetonitrile and methanol−acetonitrile mixtures with 0.6 and 0.81 mole fractions of water/methanol were studied to parallel the experimental study of Butler.[14] Briefly, the mixed solvent systems were composed of a total of 400 molecules in a tetragonal periodic cell. The BOSS program[33] automatically set up the mixed solvent systems by starting from a stored box of the pure solvent with larger molecular volume and randomly replacing the correct number of solvent molecules with molecules from the other component. All the binary solvent boxes were equilibrated at 25 °C for 100−200 million MC steps. The computed liquid densities for the solvent boxes were found to be in good agreement with the experimental values. The complete table comparing the computed and experimental densities is given in the Supporting Information as Table S1, and illustrations of all full simulation cells are given in Figures S1−S4 in the Supporting Information.

QM/MM calculations were carried out using BOSS 4.9,[33] with the reacting system treated using the semiempirical PDDG/PM3 method.[19,20,33] This combination is appropriate for a PM3-based method as it minimizes errors in computed free energies of hydration. The used QM/MM methodology allows simulation of reaction in solution on-the-fly with full sampling of the solutes by the environment. CM3 charges were obtained for the solute with a scaling factor of 1.14. This is augmented with standard Lennard-Jones interactions between solute and solvent atoms using OPLS parameters. The statistical sampling for the free energy perturbation (FEP) calculations was performed in conjunction with NPT Metropolis Monte Carlo (MC) simulations at 25 °C and 1 atm. This methodology gave the accurate results for charged and neutral species.[27−30,34] The solvent molecules were represented with the TIP4P water model[35] and the all-atom OPLS force field for acetonitrile[36] and newly developed mixed boxes. The system consisted of the reacting system plus 400 nonaqueous solvent or solvent mixture molecules, or 750 water molecules. The simulation cell was periodic and tetragonal with c/a = 1.5 where a was about 25, 29, 27, 22, 20, 28, and 28 Å for water, acetonitrile, methanol, 0.6-water−acetonitrile mixture (0.6-H_2O), 0.81-water−acetonitrile mixture (0.81-H_2O), 0.6-methanol−acetonitrile mixture (0.6-CH_3OH), and 0.81-methanol−acetonitrile mixture (0.81-CH_3OH).

To locate the minima and transition states on the free energy surfaces along the reaction pathways, two-dimensional free energy maps were constructed for each reaction using the lengths of the two transforming bonds, RC1 and RC2, as the reaction coordinates (Figure 1). The reactant state was defined by RC1 = RC2 = 5.0 Å, and the free energy surfaces were flat in this vicinity. The solvent molecules only translate and rotate, while all internal degrees of freedom for the reacting system were sampled except for the reaction coordinates. Owing to the lower acceptance rates for the large solutes in our work, the use of long MC running was needed. Each FEP calculation entailed ca. 100 million configurations of equilibration followed by 100 million configurations of averaging using increments of 0.01 Å for RC1 and RC2. Computation of the QM energy and atomic charges was performed for every attempted solute move, that is, every 100 configurations. If a MC configuration is accepted, then the QM energy, charges, and solute−solvent energies for the two perturbed solutes are also computed for the application of the Zwanzig equation.[37] Solute−solvent and solvent−solvent intermolecular cutoff distances of 12 Å were employed based on all heavy atoms of the solute, the oxygen of water and methanol, and the central carbon of acetonitrile. If any distance was within the cutoff, the entire solute−solvent or solvent−solvent interaction was included. Quadratic feathering of the intermolecular interactions within 0.5 Å of the cutoff were applied to soften the discontinuity in energy. Adjustments to the allowed ranges for rotations, translations, and dihedral angle movements led to overall acceptance rates of 30−50% and solute move acceptance rates of 3−30% for new configurations.

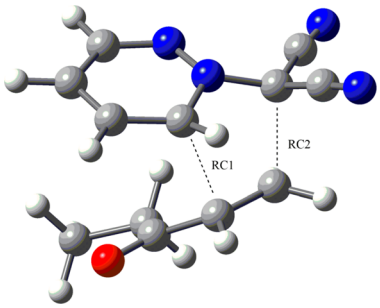

Figure 1. Reaction coordinates, RC1 and RC2, for the 1,3-dipole **1** and EVK.

The complete basis set method CBS−QB3[38] was also used to characterize the transition structures and ground states in vacuum using Gaussian 03 program.[39] In the recent study,[40] the CBS−QB3 method gave energetic results in the closest agreement to experiment for a set of 11 different pericyclic reaction compared to other ab initio and density functional theory (DFT) methods. Here, the CBS−QB3 calculations were used for geometry optimizations and computations of vibrational frequencies, which confirmed the stationary point as a minimum with all positive frequencies or as a transition state with only one imaginary frequency and provided thermodynamic corrections.

3. RESULTS AND DISCUSSION

3.1. Structures. Geometries for 1,3-dipolar cycloaddition reaction in solution were located with QM/MM/MC calculations by perturbing the distances of the two forming C−C bonds as the reaction coordinates (Figure 1). The initial ranges for RC1 and RC2 were 1.45−2.60 and 1.40−2.70 Å, respectively, with an increment of 0.05 Å to find the transition structures. The transition state was readily located, and the regions surrounding the free energy minima and maxima on the free energy surface were recomputed using increments of 0.01 Å to locate the critical points more precisely. This provided refined geometries (±0.02 Å) for the reaction in seven different solvent environments. The resultant free energy map for the reaction in 0.61H_2O−CH_3CN mixture solvent is shown in Figure 2 and required ca. 900 million single-point QM calculations per free energy map, illustrating the need for highly efficient QM methods (maps in CH_3OH, CH_3CN, and the remaining solvent mixtures are given in the Supporting Information as Figures S5−S10). All the free energy maps appear to be consistent with a stepwise mechanism with two

dx.doi.org/10.1021/jo500184f | J. Org. Chem. 2014, 79, 4863−4870

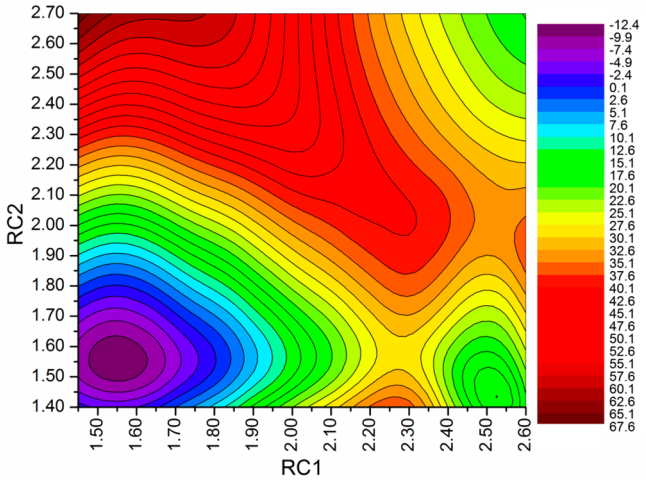

Figure 2. Two-dimensional free energy map for the 1,3-dipolar cycloaddition between **1** and EVK in 0.6-H_2O mixture. RC1 and RC2 are given in angstroms, and the relative free energy is given in kcal/mol.

transition structures TS1 and TS2, and an intermediate IM. The results are considerably different from Butler's conclusion that the reaction of **1** with EVK went through a concerted mechanism in vacuum. Previous studies have found that while the rate of the 1,3-dipolar cycloaddition reaction shows a negligible dependence on solvent polarity, product distribution can be substantially affected.[13] A possible reason for the deviation between mechanisms may greatly come from the solvent effect which plays a considerable role on the reaction.

The ability of the semiempirical PDDG/PM3 method to accurately describe the cycloaddition of **1** and EVK is certainly a concern to be addressed; hence, a gas-phase PDDG/PM3 calculation was carried out to validate the QM/MM results in a similar fashion to the two-dimensional QM/MM calculations. The resultant energy surface is given in Figure 3, and the cycloaddition reaction of **1** and EVK was found to be concerted in the gas phase. The geometrical result for the transition structure from 2-D gas-phase PDDG/PM3 FEP is listed in Table S2 (Supporting Information) along with the gas-phase

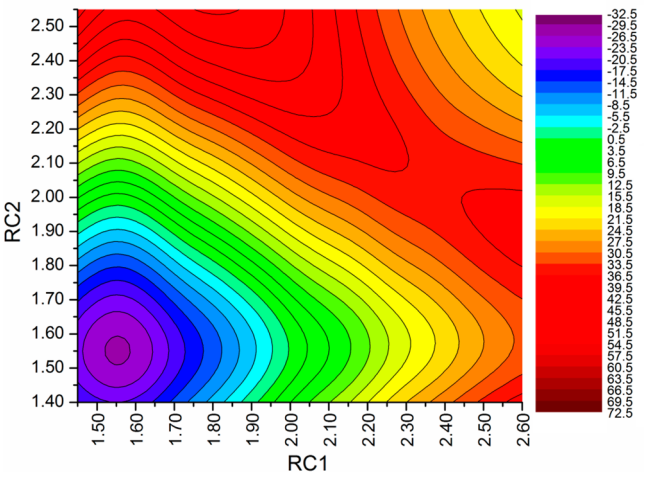

Figure 3. Two-dimensional free energy map for the 1,3-dipolar cycloaddition between **1** and EVK in the gas phase. RC1 and RC2 are given in angstroms, and the relative free energy is given in kcal/mol.

CBS-QB3 finding. It is clear that the result is in accord with the ab initio calculations. The PDDG/PM3 and CBS-QB3 results for the cycloaddition are notably similar and reflect a symmetrical, synchronous process. Thus, the semiempirical PDDG/PM3 method can accurately describe the computed reaction system. It is important to note that the current results are for the solution-phase 1,3-dipolar cycloaddition reaction, and the mechanism may still follow the concerted pathway in the gas phase.

The PDDG/PM3 geometries of the refined structures in each of the seven solvents are listed in Table 1. The rate-determining transition state, TS1, had bond distances of ca. 2.50/2.05 Å in water, CH_3OH, and all the mixture solvents, but CH_3CN had an earlier transition state at 2.51/2.10 Å. This earlier transition structure in CH_3CN is consistent with the higher activation barrier computed for IM formation relative to other solvents. The geometries for the transition structure leading to product via TS2 were found to have similar RC1 and RC2 distances in all the solvents except CH_3CN in which the geometry of the transition structure TS2 had the longest bond length. According to the results, it is obvious that the degree of bond making between **1** and EVK is less advanced in CH_3CN than in other solvents. The earlier transition structure in CH_3CN coheres with the larger activation barrier computed for product formation relative to the protic solvents.

3.2. Energetics. Activation barriers were computed for the cycloaddition reaction in solution beginning from a 5 Å separation distance for **1** and EVK. This distance was chosen to ensure an adequate separation between the reactants and avoid any possible stabilization from an exciplex complex; i.e., the free energy surfaces were flat in this vicinity. The absolute and relative free energies of activation predicted from the QM/MM/MC simulations are summarized in Table 2. Error ranges in the calculated free energy values have been estimated from fluctuations in the ΔG values for each FEP window using the batch means procedure with batch sizes of 1.0 M configurations with standard deviations of only 0.006−0.04 kcal/mol.[33] Statistical uncertainties for the free energy of activation ($\Delta G^{\ddagger}$) in TS1 were calculated to be 0.3−0.4 kcal/mol in all solvents computed.

From Table 2, the theoretical free energy of activation $\Delta G^{\ddagger}$ for TS1 are 34.4 and 30.9 kcal/mol in CH_3CN and H_2O. The experimental $\Delta G^{\ddagger}$ is 22.4 and 19.2 in CH_3CN and H_2O, respectively.[8] The calculated activation barriers are overestimated by about 11−12 kcal/mol (Table 2) compared to experimental ones. As discussed previously,[41,42] there are several issues that impact on the accuracy of the QM/MM absolute free energies of activation for bimolecular reactions. The first issue is the treatment of entropy effects in typical QM/MM simulations with either MD or MC sampling. The associated, significant entropy penalty is underestimated owing to the supposed complete sampling including full tumbling of reactants at larger separations which does not occur in the present lengthy MC runs and the fact that the vibrational energy has not been quantized and is treated classically at each MC step. The cratic entropy correction can also be estimated to decrease the entropy of activation by about 3 cal·mol^{-1}·K^{-1}. However, the largest contribution to the overestimation of the activation barriers lies in the choice of QM method. The $\Delta G^{\ddagger}$ overestimation is a systematic error common in pericyclic reactions when employing a semiempirical method.[43] For example, PDDG/PM3/MM calculations were used to study the pericyclic reaction of cyclopentadiene with different dieno-

dx.doi.org/10.1021/jo500184f | J. Org. Chem. 2014, 79, 4863−4870

Table 1. Computed Bond Lengths (Å) for the 1,3-Dipolar Cycloaddition Structures between 1 and EVK at 25 °C and 1 atm[a,b]

	H_2O	0.81-H_2O	0.6-H_2O	CH_3CN	0.6-CH_3OH	0.81-CH_3OH	CH_3OH
TS1	2.45, 2.01	2.50, 2.05	2.53, 1.99	2.51, 2.10	2.48, 2.05	2.50, 2.06	2.49, 2.07
IM	2.50, 1.46	2.51, 1.45	2.53, 2.43	2.50, 1.45	2.50, 1.44	2.51, 1.45	2.49, 1.46
TS2	2.22, 1.56	2.23, 1.53	2.27, 1.56	2.29, 1.56	2.27, 1.55	2.24, 1.57	2.27, 1.55
product	1.55, 1.55	1.55, 1.56	1.54, 1.57	1.55, 1.56	1.52, 1.55	1.55, 1.56	1.55, 1.55

[a]Figure 1. [b]RC1 and RC2 values, respectively, from the 2-D free energy maps computed in the QM/MM/MC simulations.

Table 2. Free Energy Changes, ΔG (kcal/mol), at 25 °C for the 1,3-Dipolar Cycloaddition between 1 and EVK Using QM/MM/MC

	H_2O	0.81-H_2O	0.6-H_2O	CH_3CN	0.6-CH_3OH	0.81-CH_3OH	CH_3OH
reactants	0	0	0	0	0	0	0
TS1	30.9	32.8	33.4	34.4	33.5	33.2	32.9
IM	8.9	5.5	7.1	−1.5	3.3	3.5	3.7
TS2	18.9	25.0	28.9	24.7	20.3	27.0	24.0
product	−22.0	−11.0	−11.9	−12.3	−29.2	−15.5	−14.2

philes.[31] The predicted activation barriers were considerably overestimated compared to experiment, e.g., 26.0 kcal/mol (exptl 16.0 kcal/mol) for 1,4-naphthoquinone, 32.3 kcal/mol (exptl 19.2 kcal/mol) for methy vinyl ketone, and 34.0 kcal/mol (exptl 22.2 kcal/mol) for acrylonitrile in water. These results can be taken as an indication of a poorly represented microenvironment, and higher levels of QM method are required. However, as noted above, computation of each free energy profile entailed ca. 900 million single-point QM calculations, which would make the present QM/MM approach prohibitive from a practical standpoint at the necessary ab initio levels. Though there is clearly room for improvement in the semiempirical QM methodology, it is notable that the present QM/MM/MC method reproduces well the observed rate acceleration in water over CH_3CN and methanol and provides gas-phase geometries which compare favorably to CBS−QB3 results (Table S2, Supporting Information). It is important to note that the overestimation of the absolute $\Delta G^{\ddagger}$ value is not limited to the Huisgen cycloaddition reaction, as similar errors have been reported for the Diels−Alder reaction[31,41,42,44] by Jorgensen, the Claisen rearrangement,[32] ene reaction,[45] and methyl transfer[46] using the PDDG/PM3 method. Cramer and Truhlar also reported an underestimation of the absolute rate accelerations for aqueous allyl vinyl ether and derivative Claisen rearrangements when employing the AM1 method.[47,48] However, the computed rate ratios in Figure 4 are in good agreement with the experimental observations. Since the same computational approach is used for all solvents, most errors are expected to cancel. The close agreement of the rate change indicates that solvent effects on the Huisgen cycloaddion reaction are being appropriately modeled (Table 2). Plot A in Figure 4 describes the rate relative to the rate in pure CH_3CN and shows a significant trigger point. Plot B represents the comparative influence of introducing CH_3OH instead of water into reaction of **1** with EVK, and the rate increase is more gradual with no trigger point. Further discussions between structures, solvent properties, rates, and energies are discussed in the Solvation section.

The formation of the C2−C3 bond was found to be energetically rate limiting in all solvents, and the reaction subsequently proceeded directly to a dipolar intermediate **IM** with ΔG values of 8.9, 3.7, and −1.5 kcal/mol in water, CH_3OH, and CH_3CN relative to reactants. The charge separation presented in the reactants and **IM** intermediate is

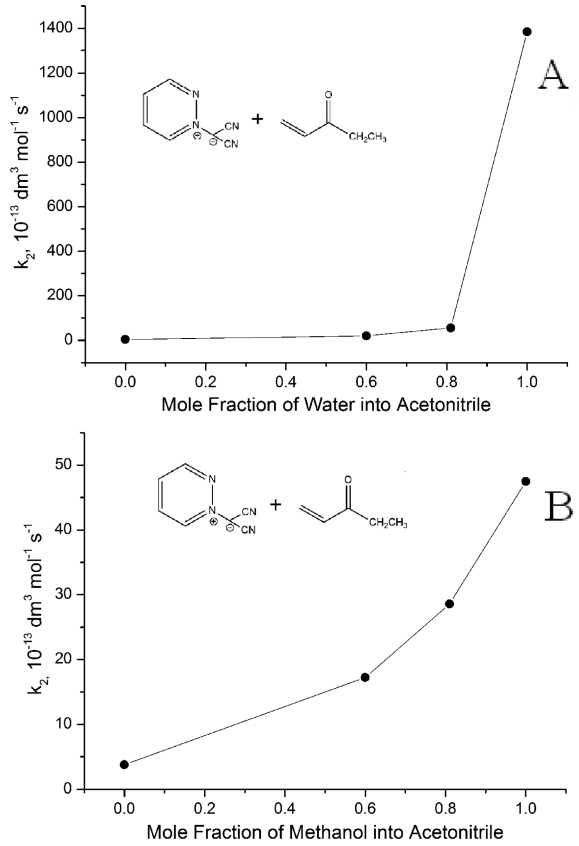

Figure 4. (A) Computed kinetic effect for the introduction of water to the 1,3-dipolar cycloaddition between **1** and EVK in acetonitrile; (B) introduction of methanol into acetonitrile.

expected to be extremely sensitive to solvent polarity and hydrogen bonding, and a direct correlation of decreasing **IM** stability with increasing solvent polarity (2.02, 46.7, and 78.4 debye for CH_3CN, CH_3OH, and water) was found (Figure 5). For the mixture solutions with same mole fraction of CH_3CN, the IM in CH_3OH−CH_3CN is more stable than in H_2O−CH_3CN. The second transition structure TS2, forming product in cycloaddition reaction, was also computed and had relative free energy values of 18.9, 24.0, and 24.7 kcal/mol to reactants in water, CH_3OH, and CH_3CN, respectively. Comparing the relative free energy from IM to TS2 yields the free energy

dx.doi.org/10.1021/jo500184f | J. Org. Chem. 2014, 79, 4863−4870

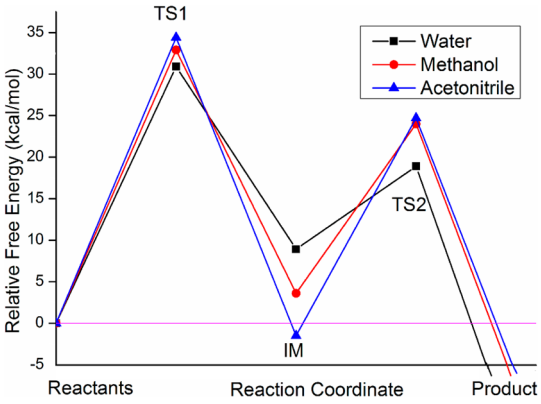

Figure 5. Free energy profiles for the 1,3-dipolar cycloaddition between **1** and EVK in three solvents from QM/MM/MC calculations.

barriers of the second step with 10.0, 20.3, and 26.2 kcal/mol in water, CH_3OH, and CH_3CN, i.e., increasing the polarity of the solvent decreases this energy barrier for the formation of RC1.

3.3. Solvation. The close agreement between the computed and observed changes in free energies of activation (Table 2) indicates that the QM/MM/MC simulations capture the origins of the medium effects at the molecular level. Specifically, the solute−solvent energy pair distributions record the average number of solvent molecules that interact with the solute and the energy associated with those interactions. The interaction energies are obtained by analyzing the results in five representative FEP windows, near the reactants, the IM intermediate, the addition and product-forming transition states, and the product. The results for the reaction in water, 0.81-H_2O mixture, and 0.6-H_2O mixture are shown in Figure 6. The solute−solvent energy pair distributions in the remaining solvents, that is, 0.8-CH_3OH, 0.61-CH_3OH, CH_3OH, and CH_3CN, can be found in the Supporting Information. Hydrogen bonding in water and CH_3OH, and the most favorable ion−dipole interactions in acetonitrile, are reflected in the left-most region with solute−solvent interaction energies more attractive than −5 kcal/mol. The band at low energy corresponds to the hydrogen bonded neighbors, and the peak near 0.0 kcal/mol is due to the wear interactions with the many distant solvent molecules located in the outer shells.

In viewing Figures 6 and S11 (Supporting Information) it is immediately clear that the intermediate and TS2 have considerably stronger energy bands in aqueous solution compared to TS1 and the reactants. The low energy bands centered around −11 kcal/mol for IM suggest a better stabilization of the strongly dipolar character of the N1 and C4 atom (see atomic numbering in Scheme 1) in aqueous solution compared to CH_3CN. The energy peak for TS1, ca. −9 kcal/mol in water, is slightly reduced compared to the intermediate.

Table 3 lists the integration of the distributions for the reactants, the transition states, the intermediate, and the product in all the solvents. The numbers of solvent are obtained by integrating the curves from 15.0 kcal/mol to −4.5 kcal/mol. Integration of the bands for the TS1, IM, and TS2 structures in CH_3CN yields 2.2, 2.3, 2.0 solvent molecules, respectively, with a large shift toward weaker interaction energies when compared to water. The strongest solute−solvent interaction is only −10 kcal/mol, and the differences between the reactants, transition states, intermediate, and

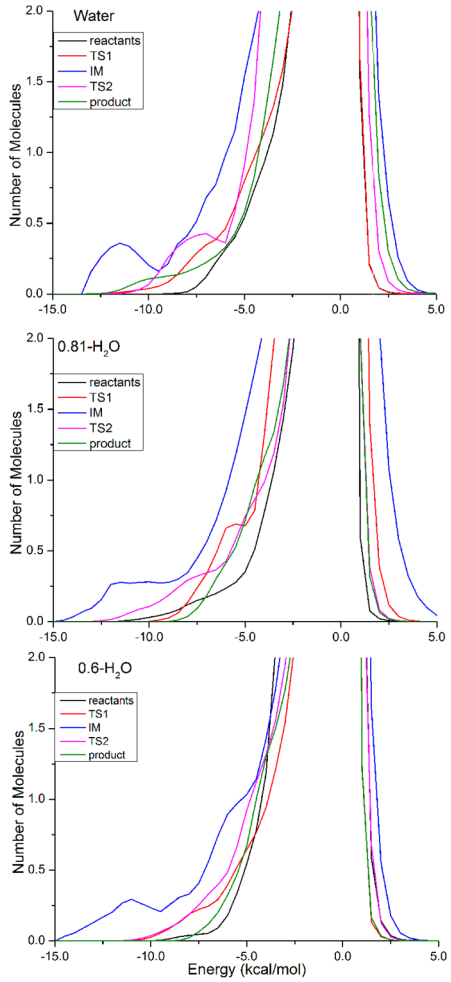

Figure 6. Solute−solvent energy pair distribution for the 1,3-dipolar cycloaddition between **1** and EVK in water, 0.81-H_2O mixture, and 0.6-H_2O mixture solvent for the reactants, transition structures (TS1 and TS2), the IM Intermediate, and the product. The ordinate records the number of solvent molecules that interact with the solutes with their interaction energy on the abscissa. Units for the ordinate are number of molecules per kcal/mol.

product are very small. The interaction from the CH_3CN solvent is simply weaker and less specific than hydrogen bonding with water. Meanwhile, those results reflect that the influence of hydrogen bond effect on the reaction energy change is quite large.

For the same molar ratio of the mixed solvents, the number of solvent is larger in H_2O−CH_3CN system than in CH_3OH−CH_3CN system. With the increase of the molar ratio of water in the mixture, the difference is also increasing. This is consistent with the difference in the reported rate of reaction which shows a gradual rate increase in CH_3OH−CH_3CN mixture, and an exponential rate enhancement in H_2O−CH_3CN mixture.

As we mentioned before, it is unclear why the difference between the performance of H_2O−CH_3CN mixture and that of CH_3OH−CH_3CN mixture can be so significant, as both H_2O and CH_3OH can form hydrogen bonds in the reaction system. The author suggested that the secondary bridging H-bonding from the first solvent shell is necessary for the exponential rate increases, and the influence of the structural feature of the alcoholic solvent on the trigger points is highly significant.

dx.doi.org/10.1021/jo500184f | J. Org. Chem. 2014, 79, 4863−4870

Table 3. Solute−Solvent Energy Pair Distribution for the 1,3-Dipolar Cycloaddition between 1 and EVK for the Reactants, the Transition States (TS1, and TS2), the Intermediate (IM), and the Product in All the Solvents Integrated to −4.5 kcal/mol

	H_2O	0.81-H_2O	0.6-H_2O	CH_3CN	0.6-CH_3OH	0.81-CH_3OH	CH_3OH
reactants	2.4	2.3	2.1	1.8	2.2	2.2	2.3
TS1	4.4	4.1	3.6	2.2	3.3	3.5	3.9
IM	14.0	8.8	7.8	2.3	6.0	6.8	9.6
TS2	5.7	4.8	4.7	2.0	4.5	4.4	4.8
product	3.7	3.2	2.9	2.1	2.6	2.8	3.0

In order to investigate the intrinsic reasons leading to this phenomenon, the solute−solvent structure for the 1,3-dipolar cycloaddition reaction in all protic solvents can be characterized by the radial distribution function, $g(R)$. Hydrogen bonding between the oxygen in dipolarophile EVK and the hydrogens of protic solvent, O (dipolarophile)−H (solvent), should yield contacts shorter than 2.5 Å. The corresponding $g_{OH}(R)$ gives the probability of finding a hydrogen of protic solvent at a distance R from the oxygen in the 1,3-dipolar cycloaddition. The reaction shows a well-defined first peak centered around 1.7 Å with a minimum around 2.5−2.7 Å. The second peak in the O (dipolarophile)−H (solvent) RDF at 3.2 Å arises from the more remote hydrogen of the linearly hydrogen-bonded protic solvent molecules. The large magnitude of the peaks for the intermediate and TS2 reflects the significantly stronger hydrogen-bonding interactions occurring compared to the reduced peak for TS1 (Figure 7). Integration of the first peaks to the minima reveals averages of 2.2/1.3 hydrogen bonds between the oxygen of the cycloaddition reaction and water/CH_3OH for the rate-limiting transition structure, TS1. However, the integration of the second peaks to the minima shows an obvious difference, which is 3.7 for water solvent and 1.4 for CH_3OH solvent. From the snapshot of TS1 in Figure 8, on average there are two short strong O···H hydrogen bonds from water molecules with the oxygen in dipolarophile. In the second solvent layer, there are four water molecules which interact with the water molecules in first solvent layer to form a large water cluster. On the other hand, there is only one CH_3OH molecule in the second solvent layer. The calculations support the fact that the growth of structured water cluster around the transition state is great important, which can well explain the experimental results.

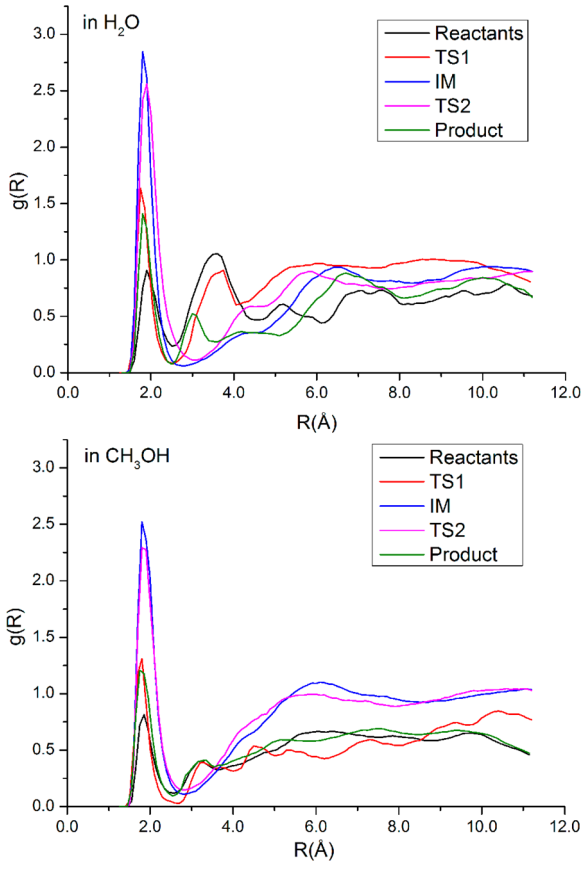

Figure 7. Computed O (in C═O of the dipolarophile)−H (water) radial distribution functions for the 1,3-dipolar cycloaddition between **1** and EVK in water and methanol at 25 °C.

3.4. Temperature. If growth of the structured water cluster around the transition state has a significant contribution to the water-induced exponential rate enhancement of the 1,3-dipolar cycloaddition reaction, raising the temperature of the reaction system should reduce the effect. As a proof of concept, the QM/MM/MC simulations at 37 °C were calculated and gave the free energies of activation of 31.8 and 34.7 kcal/mol for H_2O and CH_3CN, respectively. The resultant map for this reaction at 37 °C is shown in Figures S12 and S13 of the Supporting Information. The PDDG/PM3 results are notably similar to the results at 25 °C and reflect a stepwise mechanism.

In Figure 9, we show the effect of temperature on the rate ratio k_{water}/k_{MeCN} for the cycloaddition reaction of the dipolar **1** and EVK. The results are in good agreement with the experimental results, and there is a marked decrease in the rate enhancement in pure water. This is caused by the damage of water-structure growth. The radial distribution functions (rdfs) show a great difference, as is apparent in Figure 10. Integration of the second peak to the minima near 3.7 Å at 37 °C reveals averages of 0.8 hydrogen bonds between the dipolarphile oxygen and water molecules compared to 3.7 hydrogen bonds at 25 °C. This result can provide good support for the reported rate variations.

Although we have demonstrated that the growth of the structured water cluster around oxygen in the dipolarophile makes a great contribution to the rate enhancement between **1** and EVK, it should be noted that the growth of the structured water cluster surrounding nitrogen in the 1,3-dipole **1** can have significant influence on the rate increment. This would also extend to other 1,3-dipolar cycloaddition reactions. Using the tools presented herein, we can now analyze and rationalize the rate outcome of any given 1,3-dipolar cycloaddition reaction.

4. CONCLUSION

QM/MM/MC simulations have been carried out for 1,3-dipolar cycloaddition reaction between **1** and EVK, which has been reported through a concerted process before. However, the current solution-phase calculations using novel two-dimensional (2-D) potentials of mean force present an

dx.doi.org/10.1021/jo500184f | J. Org. Chem. 2014, 79, 4863−4870

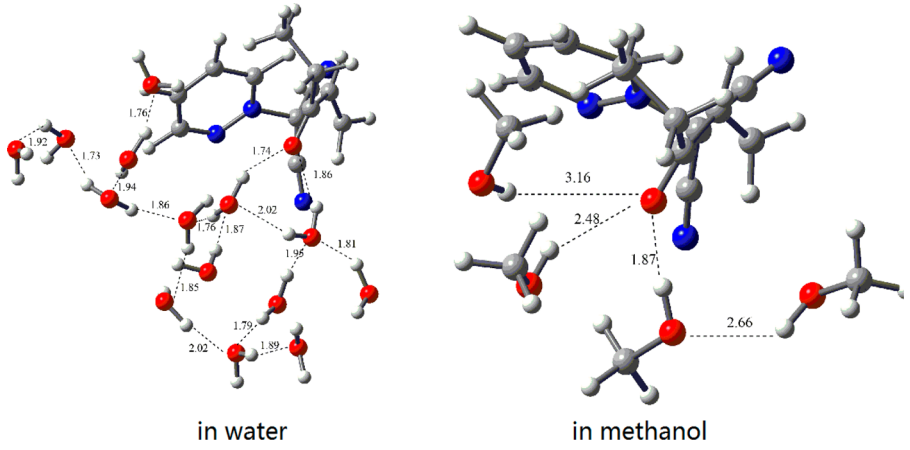

Figure 8. Typical snapshot for the rate-limiting transition structure, TS1 from the 1,3-dipolar cycloaddition between **1** and EVK in water and methanol (only nearest solvent molecules are illustrated). Distances in angstroms.

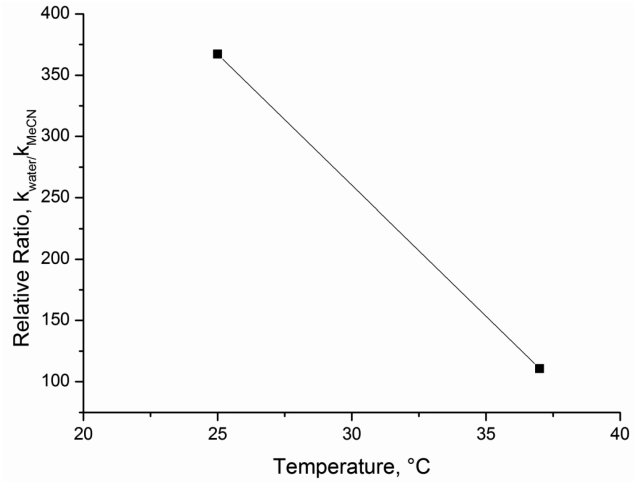

Figure 9. Influence of temperature on the ratio k_{H2O}/k_{MeCN} for the 1,3-dipolar cycloaddition between **1** and EVK.

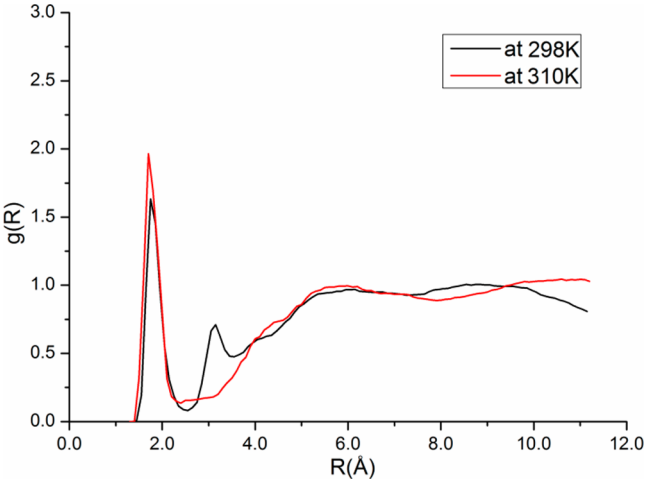

Figure 10. Computed O (in C═O of the dipolarophile)−H (water) radial distribution functions for the 1,3-dipolar cycloaddition between **1** and EVK in water.

alternative potential energy surface which supports a stepwise mechanism interpretation. The current study has provide further insight into the effect of solvent on the 1,3-dipolar cycloaddition reaction through energy pair distributions, radial distribution functions, and changes in charges along the reaction pathway. The most significant solvent effect reported is the change in the reaction pathway from the concerted mechanism to a stepwise reaction.

In conclusion, the results of the theoretical calculations support the implication from the experimental results that the growth of structured water clusters around the transition state has a significant effect on the exponential rate enhancement. The studies presented herein have revealed the crucial importance of solvent effect in this chemistry and may have a significant impact on other computationally derived PESs featuring the influence of solvent.

■ ASSOCIATED CONTENT

Ⓢ Supporting Information

Computed and experimental densities for mixture solvents; illustration of the full simulation mixture solvent cells; additional two-dimensional potential of mean force (free energy map); additional solute−solvent energy pair distributions; coordinates of transition structure computed using CBS−QB3 methods. This material is available free of charge via the Internet at http://pubs.acs.org.

■ AUTHOR INFORMATION

Corresponding Author

*E-mail: yxue@scu.edu.cn. Tel: +86 28 85418330.

Notes

The authors declare no competing financial interest.

■ ACKNOWLEDGMENTS

This project has been supported by the National Natural Science Foundation of China (Grant No. 21173151) and by the National Basic Research Program of China (973 Program, 2011CB201202) of the Ministry of Science and Technology of China (MOST).

■ REFERENCES

(1) Rideout, D. C.; Breslow, R. *J. Am. Chem. Soc.* **1980**, *102*, 7816.
(2) Breslow, R. *Acc. Chem. Res.* **1991**, *24*, 159.
(3) Engberts, J. B. F. N.; Blandamer, M. J. *Chem. Commun.* **2001**, 1701.
(4) Cave, G. W. V.; Raston, C. L.; Scott, J. L. *Chem. Commun.* **2001**, 2159.

(5) Biscoe, M. R.; Breslow, R. *J. Am. Chem. Soc.* **2003**, *125*, 12718.
(6) Padwa, A.; Pearson, W. H. *Synthetic Applications of 1,3-Dipolar Cycloaddition Chemistry toward Heterocycles and Natural Products*; Wiley & Sons: Hoboken, 2003; Vol. *59*.
(7) Milosevic, S.; Togni, A. *J. Org. Chem.* **2013**, *78*, 9638.
(8) Li, Y.-J.; Huang, H.-M.; Dong, H.-Q.; Jia, J.-H.; Han, L.; Ye, Q.; Gao, J.-R. *J. Org. Chem.* **2013**, *78*, 9424.
(9) Diz, P. M.; Coelho, A.; El Maatougui, A.; Azuaje, J.; Caamaño, O.; Gil, Á.; Sotelo, E. *J. Org. Chem.* **2013**, *78*, 6540.
(10) Morozov, D. A.; Kirilyuk, I. A.; Komarov, D. A.; Goti, A.; Bagryanskaya, I. Y.; Kuratieva, N. V.; Grigor'ev, I. A. *J. Org. Chem.* **2012**, *77*, 10688.
(11) Basch, C. H.; Brinck, J. A.; Ramos, J. E.; Habay, S. A.; Yap, G. P. A. *J. Org. Chem.* **2012**, *77*, 10416.
(12) Li, X.; Liu, B.; Yu, X.; Yi, P.; Yi, R.; Chmielewski, P. J. *J. Org. Chem.* **2012**, *77*, 2431.
(13) Butler, R. N.; Coyne, A. G.; Cunningham, W. J.; Burke, L. A. *J. Chem. Soc., Perkin Trans. 2* **2002**, 1807.
(14) Butler, R. N.; Cunningham, W. J.; Coyne, A. G.; Burke, L. A. *J. Am. Chem. Soc.* **2004**, *126*, 11923.
(15) R. Gholami, M.; Habibi Yangjeh, A. *J. Chem. Res., Synop.* **1999**, 226.
(16) Aaqvist, J.; Warshel, A. *Chem. Rev.* **1993**, *93*, 2523.
(17) Gao, J. *Acc. Chem. Res.* **1996**, *29*, 298.
(18) Kaminski, G. A.; Jorgensen, W. L. *J. Phys. Chem. B* **1998**, *102*, 1787.
(19) Repasky, M. P.; Chandrasekhar, J.; Jorgensen, W. L. *J. Comput. Chem.* **2002**, *23*, 1601.
(20) Tubert-Brohman, I.; Guimarães, C. R. W.; Repasky, M. P.; Jorgensen, W. L. *J. Comput. Chem.* **2004**, *25*, 138.
(21) Tubert-Brohman, I.; Guimarães, C. R. W.; Jorgensen, W. L. *J. Chem. Theory Comput.* **2005**, *1*, 817.
(22) Kostal, J.; Jorgensen, W. L. *J. Am. Chem. Soc.* **2010**, *132*, 8766.
(23) Acevedo, O.; Jorgensen, W. L.; Evanseck, J. D. *J. Chem. Theory Comput.* **2006**, *3*, 132.
(24) Armacost, K.; Acevedo, O. *J. Am. Chem. Soc.* **2013**, *136*, 147.
(25) Allen, C.; Sambasivarao, S. V.; Acevedo, O. *J. Am. Chem. Soc.* **2012**, *135*, 1065.
(26) Alexandrova, A. N.; Jorgensen, W. L. *J. Phys. Chem. B* **2011**, *115*, 13624.
(27) Vayner, G.; Houk, K. N.; Jorgensen, W. L.; Brauman, J. I. *J. Am. Chem. Soc.* **2004**, *126*, 9054.
(28) Acevedo, O.; Jorgensen, W. L. *Org. Lett.* **2004**, *6*, 2881.
(29) Acevedo, O.; Jorgensen, W. L. *J. Am. Chem. Soc.* **2005**, *127*, 8829.
(30) Acevedo, O.; Jorgensen, W. L. *J. Org. Chem.* **2006**, *71*, 4896.
(31) Thomas, L. L.; Tirado-Rives, J.; Jorgensen, W. L. *J. Am. Chem. Soc.* **2010**, *132*, 3097.
(32) Acevedo, O.; Armacost, K. *J. Am. Chem. Soc.* **2010**, *132*, 1966.
(33) Jorgensen, W. L.; Tirado-Rives, J. *J. Comput. Chem.* **2005**, *26*, 1689.
(34) Acevedo, O.; Jorgensen, W. L. *J. Am. Chem. Soc.* **2006**, *128*, 6141.
(35) Jorgensen, W. L.; Chandrasekhar, J.; Madura, J. D.; Impey, R. W.; Klein, M. L. *J. Chem. Phys.* **1983**, *79*, 926.
(36) Jorgensen, W. L.; Maxwell, D. S.; Tirado-Rives, J. *J. Am. Chem. Soc.* **1996**, *118*, 11225.
(37) Zwanzig, R. W. *J. Chem. Phys.* **1954**, *22*, 1420.
(38) Ochterski, J. W.; Petersson, G. A.; Montgomery, J. A. *J. Chem. Phys.* **1996**, *104*, 2598.
(39) Frisch, M. J.; Trucks, G. W.; Schlegel, H. B.; Scuseria, G. E.; Robb, M. A.; Cheeseman, J. R.; Montgomery, J. A., Jr.; Vreven, T.; Kudin, K. N.; Burant, J. C.; Millam, J. M.; Iyengar, S. S.; Tomasi, J.; Barone, V.; Mennucci, B.; Cossi, M.; Scalmani, G.; Rega, N.; Petersson, G. A.; Nakatsuji, H.; Hada, M.; Ehara, M.; Toyota, K.; Fukuda, R.; Hasegawa, J.; Ishida, M.; Nakajima, T.; Honda, Y.; Kitao, O.; Nakai, H.; Klene, M.; Li, X.; Knox, J. E.; Hratchian, H. P.; Cross, J. B.; Bakken, V.; Adamo, C.; Jaramillo, J.; Gomperts, R.; Stratmann, R. E.; Yazyev, O.; Austin, A. J.; Cammi, R.; Pomelli, C.; Ochterski, J. W.; Ayala, P. Y.; Morokuma, K.; Voth, G. A.; Salvador, P.; Dannenberg, J. J.; Zakrzewski, V. G.; Dapprich, S.; Daniels, A. D.; Strain, M. C.; Farkas, O.; Malick, D. K.; Rabuck, A. D.; Raghavachari, K.; Foresman, J. B.; Ortiz, J. V.; Cui, Q.; Baboul, A. G.; Clifford, S.; Cioslowski, J.; Stefanov, B. B.; Liu, G.; Liashenko, A.; Piskorz, P.; Komaromi, I.; Martin, R. L.; Fox, D. J.; Keith, T.; Al-Laham, M. A.; Peng, C. Y.; Nanayakkara, A.; Challacombe, M.; Gill, P. M. W.; Johnson, B.; Chen, W.; Wong, M. W.; Gonzalez, C.; Pople, J. A. *Gaussian 03*; Gaussian, Inc.: Wallingford, CT, 2003.
(40) Guner, V.; Khuong, K. S.; Leach, A. G.; Lee, P. S.; Bartberger, M. D.; Houk, K. N. *J. Phys. Chem. A* **2003**, *107*, 11445.
(41) Chandrasekhar, J.; Shariffskul, S.; Jorgensen, W. L. *J. Phys. Chem. B* **2002**, *106*, 8078.
(42) Acevedo, O.; Jorgensen, W. L. *J. Chem. Theory Comput.* **2007**, *3*, 1412.
(43) Sattelmeyer, K. W.; Tubert-Brohman, I.; Jorgensen, W. L. *J. Chem. Theory Comput.* **2006**, *2*, 413.
(44) Acevedo, O.; Jorgensen, W. L.; Evanseck, J. D. *J. Chem. Theory Comput.* **2007**, *3*, 132.
(45) Sheppard, A. N.; Acevedo, O. *J. Am. Chem. Soc.* **2009**, *131*, 2530.
(46) Gunaydin, H.; Acevedo, O.; Jorgensen, W. L.; Houk, K. N. *J. Chem. Theory Comput.* **2007**, *3*, 1028.
(47) Cramer, C. J.; Truhlar, D. G. *J. Am. Chem. Soc.* **1992**, *114*, 8794.
(48) Cramer, C. J.; Truhlar, D. G. *Science* **1992**, *256*, 213.